Organic & Biomolecular Chemistry

www.rsc.org/obc

Volume 7 | Number 18 | 21 September 2009 | Pages 3613–3880

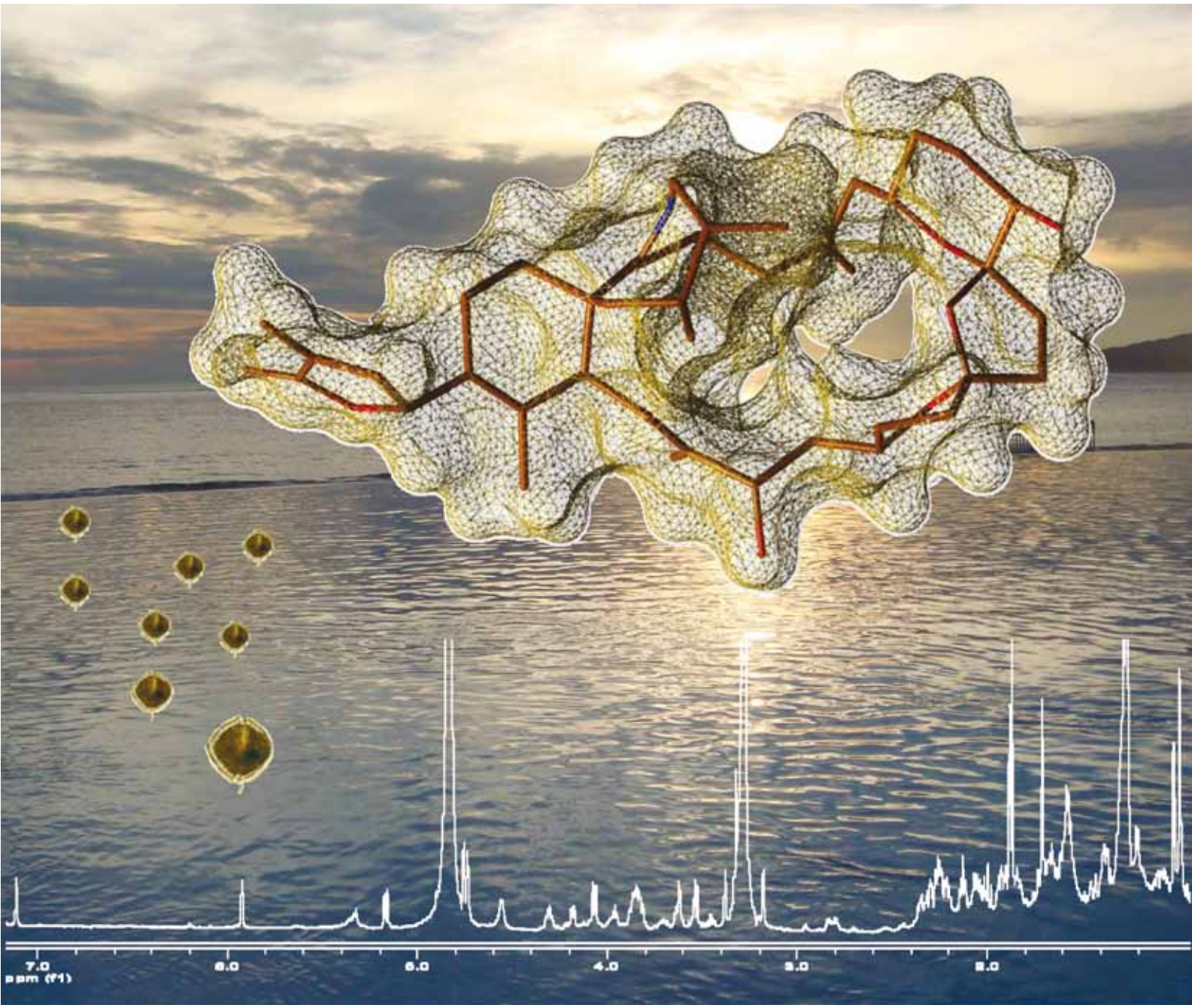

ISSN 1477-0520

RSC Publishing

FULL PAPER

Patrizia Ciminiello *et al.*
Full relative stereochemistry assignment and conformational analysis of 13,19-didesmethyl spirolide C

Highlights in
Chemical Science

In this issue

1477-0520(2009)7:18;1-9

Full relative stereochemistry assignment and conformational analysis of 13,19-didesmethyl spirolide C *via* NMR- and molecular modeling-based techniques. A step towards understanding spirolide's mechanism of action†

Patrizia Ciminiello, Bruno Catalanotti, Carmela Dell'Aversano, Caterina Fattorusso, Ernesto Fattorusso, Martino Forino,* Laura Grauso, Angela Leo and Luciana Tartaglione

Received 16th April 2009, Accepted 17th June 2009
First published as an Advance Article on the web 16th July 2009
DOI: 10.1039/b907649b

The relative stereochemistry of 13,19-didesmethyl spirolide C was determined through careful analysis of NMR parameters strongly dependent upon molecular conformations supported and extended by computational studies. This work has also shed light on the conformational behavior of spirolides in solution. An equilibrium between two possible conformers of the identified diastereoisomer was inferred, while the uncommon cyclic imine moiety of spirolides—the putative pharmacophore of this class of toxins—was interestingly found to adopt only a single dominant conformation. The insightful details provided on spirolide conformations may represent a key means to pharmacologists involved in clarifying the mechanism of action of spirolide, which is yet to be totally defined.

1. Introduction

Since the end of 2003, massive blooms of the toxic dinoflagellate *Alexandrium ostenfeldii* have been detected across the Northern Adriatic Sea, where over the past few years it has represented the major harmful alga affecting shellfish consumers' health as well as aquaculture economy.[1]

Coinciding with the surge of *A. ostenfeldii* in the Adriatic Sea, our group undertook a research program aimed at defining the toxin profile of this dinoflagellate that was eventually found to produce a relatively large number of spirolides. Among them, three major compounds were unambiguously identified as 13-desmethyl spirolide C[2] (**1**), 13,19-didesmethyl spirolide C[3] (**2**), and 27-hydroxy-13,19-didesmethyl spirolide C[4] (**3**), the latter being a previously unreported spirolide (Fig. 1). In addition, several minor spirolides were also detected, for all of which, though, only preliminary mass-based structural hypotheses were ventured, as they had been isolated in amounts that were too small for NMR investigations.[4]

Spirolides are referred to as fast-acting toxins, since they induce rapid onset of symptoms akin to those reported for the acute toxicity of paralytic shellfish poisoning (PSP) toxins, followed by death within minutes, as demonstrated by intraperitoneal injection into a mouse.[5] It has been shown that spirolides affect Ca^{2+} channels[6] and hypothesized that their pharmacophore is represented by the uncommon cyclic imine moiety.[7] Apart from the above toxicological and pharmacological data, the spirolide mechanism of action remains largely undisclosed.

Dipartimento di Chimica delle Sostanze Naturali, Università di Napoli "Federico II", via D. Montesano, 49, 80131 Napoli, Italy. E-mail: forino@unina.it

† Electronic supplementary information (ESI) available: Conformational search results analysis: graph depicting rate of 4*R*,19*R* conformers (Fig. S1); classification into families and geometric parameters relative to the THF-pyranose moiety of 4*R*,19*S* and 4*R*,19*R* diastereoisomers (Table S1); classification into families and geometric parameters of 4*R*,19*R* diastereoisomer (Table S2). See DOI: 10.1039/b907649b

In order to clarify the molecular basis of spirolide biological activity, we decided to investigate the stereochemistry and conformational space of this intriguing class of marine biotoxins. In particular, we focused our attention on 13,19-didesmethyl spirolide C, since we had isolated it in relatively large amount.[4]

With regard to the stereochemistry of spirolides, so far only the relative stereochemistry of 13-desmethyl spirolide C, together with those of spirolides B and D, has been determined, devoid, though, of configuration at C4.[8]

In this paper, we report on a combination of NMR and molecular modeling studies that led to the determination of the full relative stereochemistry of 13,19-didesmethyl spirolide C.

NMR coupling constant values and ROESY cross-peaks were also employed as a guide in the molecular modeling investigation with the purpose of detecting the most abundant conformations of 13,19-didesmethyl spirolide C in solution.

2. Results and discussion

2.1 Relative stereochemistry assignment of 13,19-didesmethyl spirolide C

The relative stereochemistry of 13,19-didesmethyl spirolide C (**2**) was mostly assigned on the basis of the reported relative stereochemistry of 13-desmethyl spirolide C (**1**), which had been elucidated at all of its chiral centers except C4.[8] Considering that the ^{1}H and ^{13}C chemical shifts of **2** mostly overlapped those of **1** (Table 1), we could assume that the two molecules had the same stereochemistry at all the chiral centers apart from C19, where **1** and **2** are substituted differently. Hence, for assigning the full relative stereochemistry of 13,19-didesmethyl spirolide C, we had to elucidate configurations at C4 and C19. Initially, we resorted to interpreting some NMR parameters strongly dependent upon molecular conformations, such as proton–proton vicinal coupling constants ($^{3}J_{H\text{-}H}$), carbon–proton vicinal coupling constants

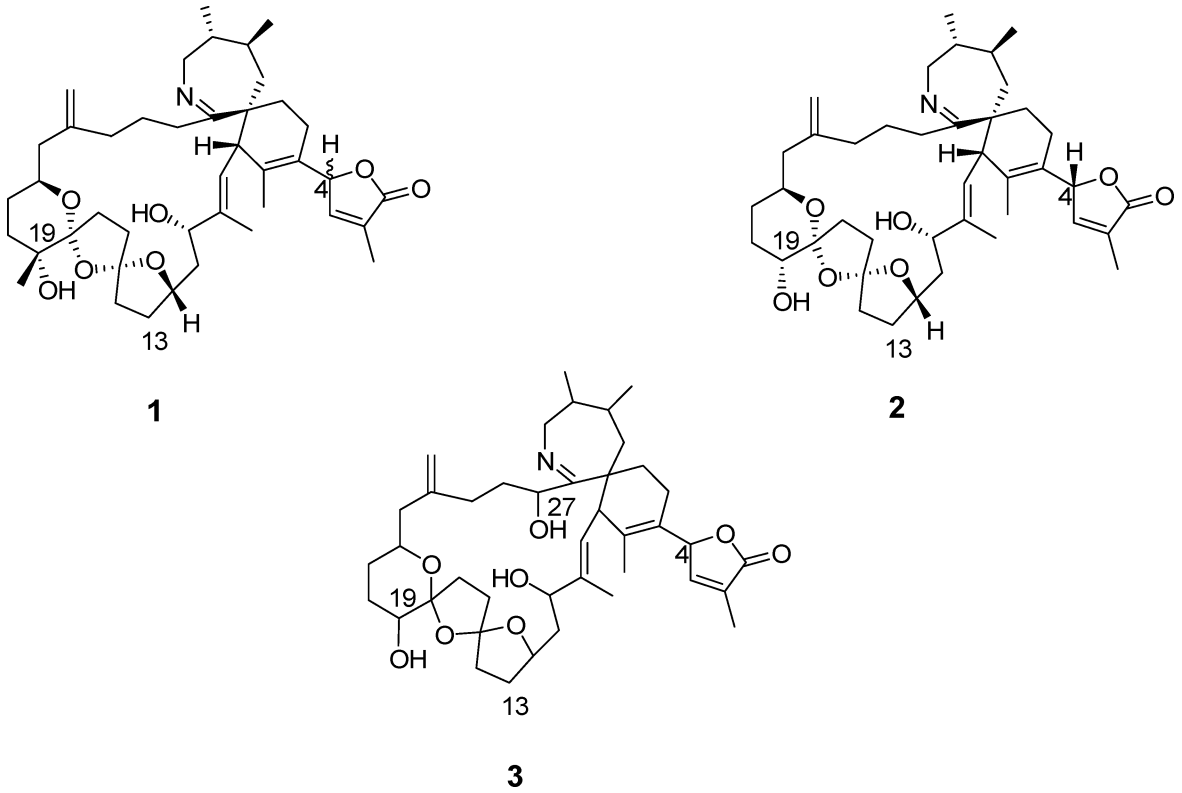

Fig. 1 Stereostructure of 13-desmethyl spirolide C (**1**) devoid of configuration at C4; full stereostructure of 13,19-didesmethyl spirolide C (**2**); planar structure of 27-hydroxy-13,19-didesmethyl spirolide C (**3**).

($^3J_{C\text{-}H}$), and spatial proximity of hydrogen nuclei (ROESY correlations). These NMR data guided the molecular modeling analysis that was performed employing the relative configuration of previously determined chiral centers depicted in Fig. 2. The four possible diastereoisomers derived from the combination of *R* and *S* configurations at C4 and C19 (namely 4*R* 19*R*, 4*R* 19*S*, 4*S* 19*R*, and 4*S* 19*S*) were subjected to a conformational search using a combination of molecular dynamics (MD) and molecular mechanic (MM) calculations. The resulting conformers were subjected to quantum mechanic (QM) full geometry optimization through the semiempirical method AM1. All the obtained MM and AM1 conformers were ranked on the basis of their conformational energy values, grouped into families according to the values of selected dihedral angles (see Experimental), and finally evaluated in the light of the NMR data (Table 2, Table 3, and Table 4; Table S1, Table S2, and Fig. S1 in the ESI†).

Such a study not only allowed us to define the stereochemistry at C4 and C19, respectively, but it also provided crucial information about the dominant conformations assumed by 13,19-didesmethyl spirolide C in solution.

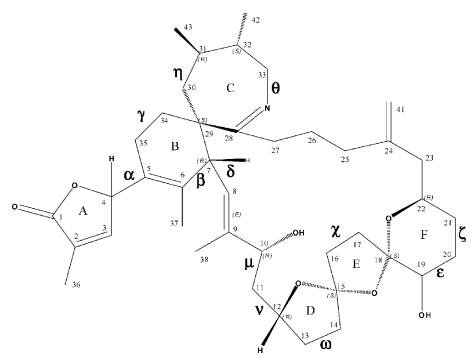

Fig. 2 Stereostructure of 13,19-didesmethyl spirolide C (**2**). Configuration of previously determined chiral centers is reported. Rotatable bonds used for structural classification into families are indicated with Greek letters.

2.2 C4 stereochemistry assignment

In order to elucidate the configuration at C4, we started out by analyzing the carbon–proton vicinal coupling constants ($^3J_{C\text{-}H}$). Small values of $^3J_{C\text{-}H}$ between H4 and C6 (1.8 Hz) as well as between H4 and C35 (0 Hz) brought to light the existence of a dominant conformer around the C4–C5 bond characterized by a gauche relationship between H4 and both C6 and C35.

At this point, a conformational search was performed as described in the previous section.

The obtained molecular modeling-based results were analyzed in order to investigate possible orientations of the unsaturated lactone (moiety A) with respect to the cyclohexene ring B, crucial for the C4 stereochemical assignment. To this aim, the value of the dihedral angle α (H4–C4–C5–C6; Fig. 2) was measured in all of the obtained conformers. AM1 conformers showed three possible values of α (Table 2): one corresponding to an *anti* orientation of H4 with respect to C6, which was ruled out on the basis of the experimentally ascertained H4/C6 gauche-like orientation—and

Table 1 ^{1}H and ^{13}C Chemical Shifts of 13-desmethylspirolide C (**1**) and 13,19-didesmethylspirolide C (**2**)

	1		**2**	
Position	δ_H	δ_C	δ_H	δ_C
1	—	176.8	—	176.5
2	—	131.0	—	130.6
3	7.12	149.5	7.12	149.6
4	5.95	82.0	5.94	82.5
5	—	126.4	—	125.8
6	—	134.7	—	134.1
7	3.56	48.1	3.59	48.5
8	5.16	124.2	5.16	125.1
9	—	144.6	—	143.8
10	4.15	76.8	4.06	77.2
11	1.37;2.25	45.2	1.36;2.32	45.7
12	4.30	79.8	4.31	80.0
13	1.70;2.27	32.8	1.70;2.26	32.3
14	1.95;2.29	38.2	1.95;2.28	37.8
15	—	118.1	—	117.8
16	2.07;2.21	35.2	2.05;2.12	35.2
17	**1.79;2.20**	**32.1**	**1.91;2.21**	**34.5**
18	**–**	**112.2**	**–**	**109.4**
19	**–**	**71.1**	**3.33**	**72.0**
20	**1.49;1.81**	**35.7**	**1.59;1.67**	**29.4**
21	**1.28;1.58**	**29.9**	**1.11;1.65**	**31.0**
22	3.97	69.1	3.90	69.5
23	2.06;2.41	46.3	2.00;2.31	47.0
24	—	147.8	—	147.1
25	1.58;2.10	36.0	1.55;2.11	35.9
26	1.40;2.02	23.4	1.39;2.00	23.2
27	2.32;2.32	35.6	2.35;2.35	35.7
28	—	178.6	—	178.0
29	—	50.8	—	51.2
30	1.55;1.73	38.3	1.54;1.73	37.9
31	1.16	36.9	1.08	37.0
32	1.36	41.2	1.39	41.1
33	3.44;3.76	53.3	3.45;3.80	52.9
34	1.52;1.80	32.4	1.47;1.79	32.0
35	1.51;2.14	20.3	1.52;2.12	20.1
36	1.90	10.4	1.88	10.5
37	1.72	17.1	1.71	17.2
38	1.87	12.3	1.86	12.2
39	—	—	—	—
40	—	22.7	1.19	—
41	4.73;4.76	111.3	4.75;4.78	110.8
42	1.03	18.9	0.98	19.7
43	1.00	20.1	0.95	20.4

^{1}H chemical shifts were derived from a z-TOCSY experiment. ^{13}C chemical shifts were determined through ^{1}H-^{13}C HSQC and psHMBC experiments. ^{1}H and ^{13}C values significantly differing in **1** and **2** are reported in bold.

two corresponding to a *gauche*-like orientation (namely, *gauche*$^-$ $\alpha \sim -50°$ and *gauche*$^+$ $\alpha \sim +50°$; Table 2).

At this point, we could discriminate between the two *gauche*-like orientations relying on z-TOCSY and ROESY experiments.

Table 2 Dihedral angle α values and related intramolecular distances measured on AM1 conformers of 4*R* and 4*S* diastereoisomers

Family	Dihedral angle α (°)	H3–H37 (Å)	H4–H37 (Å)	H4–H35a (Å)
4*R*				
anti	168°	3.3	3.8	2.5
gauche$^-$	–53°	2.5	2.1	3.3
gauche$^+$	43°	4.7	2.3	3.7
4*S*				
anti	–176°	3.4	3.7	2.2
gauche$^+$	39°	2.3	2.3	3.7
gauche$^-$	–41°	4.2	2.4	3.7

Firstly, analysis of multiplicity relative to $H_2$34, $H_2$35, and $H_2$30—extrapolated from the z-TOCSY experiment—led us to assign a *pseudo*-equatorial orientation to H30a, H34b, and H35a as well as a *pseudo*-axial orientation to H30b, H34a, and H35b (Fig. 3). Such information was decisive for properly interpreting the ensuing key ROESY cross-peaks: H4/H35a, $CH_3$37/H3, $CH_3$37/H4, and H3/H30a. These correlations allowed us to draw the following conclusions: (i) H3 had to be spatially close to $CH_3$37; (ii) H4, $CH_3$37, and H35a had to lie on the same side of the molecule, with H4 closer to $CH_3$37 than to H35a, as suggested by the relative ROE strengths (Table 5). Therefore, we could conclude that only the *gauche*$^-$ conformer of the diastereoisomers with *R* configuration at C4 ($\alpha = -53°$; Table 2, Fig. 4) featured a relative atomic orientation totally consistent with all of the experimental data. In fact, 4*S* *gauche*-like orientation was not compatible with the observed ROE between H4 and H35a.

In conclusion, the combination of molecular modeling studies and NMR data allowed to unambiguously assign *R* configuration at C4 ($\alpha = -53°$; Table 2, Fig. 4).

2.3 C19 stereochemistry assignment

Assignment of configuration at C19 was achieved through applying the same NMR- and molecular modeling-based approach discussed for the C4 stereochemistry elucidation. First of all, the conformational behavior of rings E and F, respectively, was investigated. Conformers obtained by QM semiempirical (AM1) geometry optimization showed a unique quasi-planar conformation of ring E, which was not in agreement with the X-ray determined tetrahydrofuran (THF)-ring pseudoration reported for THF-spiro systems.[9] Therefore, we decided to test various QM semiempirical and empirical (MM) alike. In accordance with some previously reported data[9], we found that QM semiempirical methods yielded conformers with flatter geometries than those obtained by MM methods, thus proving less accurate in reproducing the experimentally determined geometry of THF-spiro

Table 3 MM conformers within 5 kcal/mol from the global minimum of 4*R*19*S* and 4*R*19*R* diasteroisomers grouped into families according to dihedral angle values of rings E and F. Inter-atomic distances determinant for C19 stereochemistry assignment are reported

Family	ΔE_{GM} (Kcal/mol)	ε (°)	ζ (°)	χ (°)	H19–H′21 (Å)	H19–H″21 (Å)	H17b–H19 (Å)	H12–H16a (Å)
19*R*								
A1	0.0	–54	53	32	2.6	3.8	3.5	3.6
A2	1.4	–52	52	–22	2.6	3.8	2.9	3.7
19*S*								
A1	1.8	–53	52	38	3.9	4.3	3.9	3.0
A2	0.0	–52	53	–39	3.9	4.3	3.7	3.7

Table 4 MM conformers of 4*R*19*R* diasteroisomer grouped into families according to geometric parameters. Lowest energy conformers of each family within 5 kcal/mol from the global minimum are reported

		Dihedral angle values (°)										
Family	ΔE_{GM} (Kcal/mol)	β	γ	θ	η	ε	ζ	χ	ω	δ	μ	ν
I	0.0	20	–41	64	–154	–54	53	32	40	–123	159	–62
II	1.4	19	–42	64	–154	–52	52	–22	41	–122	171	–62
III	2.2	23	–39	–53	–174	–54	52	30	35	–116	160	–65
IV	2.8	24	–36	65	–154	–53	52	33	–39	–126	166	–61
V	3.3	22	–40	68	–154	–52	54	–40	24	–121	74	58
VI	3.4	9	–47	–54	79	–52	53	–40	25	–104	–82	–179
VII	3.6	24	–35	–47	83	–53	52	–24	40	–124	175	–59
VIII	3.7	28	–37	53	–177	–53	53	–26	41	–127	176	–53
IX	4.0	6	–48	62	–154	–54	53	–41	32	–112	–85	–176
X	4.1	28	–36	–51	–171	–53	54	35	–33	–117	–174	–53
XI	4.3	24	–36	–48	83	–53	52	24	39	–125	166	–64
XII	4.6	24	–38	–54	–175	–53	54	–35	34	–122	–91	–172
XIII	4.6	17	–43	–56	–176	–55	52	–41	27	–123	–77	173
XIV	4.7	18	–42	64	–154	–53	52	32	40	–121	–109	179
XV	4.7	21	–41	65	–155	–52	52	34	38	–126	–77	–152
XVI	4.9	27	–36	–52	–172	–53	52	34	39	–113	–108	179
XVII	4.9	23	–38	55	69	–52	54	–40	14	–123	–79	176

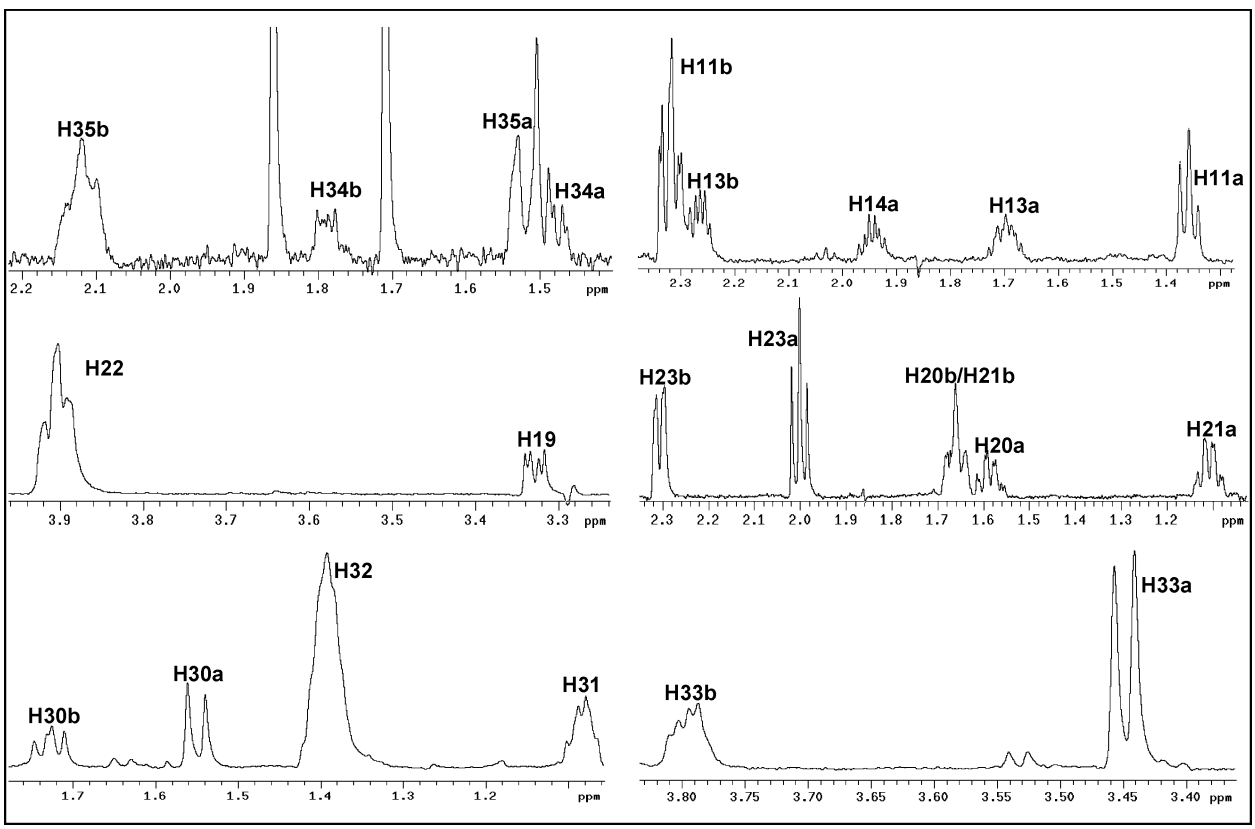

Fig. 3 Selected multiplicity of protons crucial for stereochemical assignment of 13,19-didesmethyl spirolide C. 1D-NMR projections have been extrapolated from a z-filtered TOCSY experiment.

systems. Consequently, only MM conformers having the assigned *R* configuration at C4 (namely, 4*R* 19*R* and 4*R* 19*S*) were taken into account for the analysis of possible conformations of rings E and F, respectively. All of the obtained conformers were then ranked on the basis of their conformational energy values and grouped into families according to the values of dihedral angles ε (C18–C19–C20–C21), ζ (C19–C20–C21–C22), and χ (C15–C16–C17–C18) (Fig. 2). Our analyses showed that ring F had the same strong conformational preference in both the selected diastereoisomers (4*R* 19*R* and 4*R* 19*S*), corresponding to the chair depicted in Fig. 5 and characterized by values of dihedral angles ε and ζ (Fig. 2) around –50° and +50°, respectively (Table 3). This conformation of ring F was found in all of the conformers within 5 kcal/mol from the global minimum (Fig. S1 in the ESI†) and represented 77.0% of all of the 4*R* 19*R* conformers and 71.5% of all of the 4*R* 19*S* conformers, respectively (Table S1 in the

Table 5 Strengths of ^{1}H-^{1}H ROESY cross peaks for 13,19-didesmethyl spirolide C (**2**) in CD_3OD

Proton A	Proton B	ROE strength
H3	H37	weak
H3	H30a	very weak
H4	H37	strong
H4	H35a	very weak
H7	H38	strong
H7	H34a	weak
H8	H10	medium
H8	H31	weak
H8	H43	medium
H10	H13a	weak
H10	H13b	very weak
H10	H14b	very weak
H11a	H22	very weak
H12	H13b	weak
H12	H14a	very weak
H12	H16a	very weak
H13a	H14b	strong
H13b	H14a	strong
H16a	H17b	medium
H16b	H17a	weak
H17b	H19	weak
H19	H21a	weak
H20a	H22	very weak
H30a	H31	very weak
H30b	H33b	weak
H30b	H32	weak
H32	H33b	weak
H32	H33a	weak
H32	H43	medium
H33a	H42	medium
H33b	H34b	medium
H34b	H35b	very weak

Cross-peaks were subdivided into 'strong', 'medium', 'weak', and 'very weak' based on the relative peak heights.

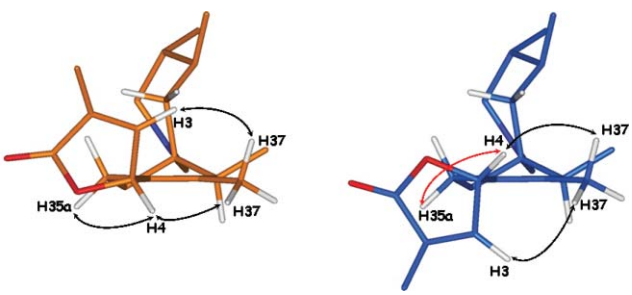

Fig. 4 Comparison of the *gauche*$^{-}$ conformer of 4*R* (left, orange carbons) with the *gauche*$^{+}$ conformer of 4*S* (right, cyan carbons). Black arrows indicate possible ROEs, red arrows indicate impossible ROEs.

ESI†). In our opinion, such a strong conformational preference may be caused either by unfavorable coulomb interactions between oxygens present in rings E and F, or by an H-bond between the hydroxyl group at C19 and the oxygen in ring E.

Eventually, only the 4*R* 19*R* diastereoisomer presented stereochemical features fully consistent with the NMR data suggesting an axial position for both H19 and H21a (Fig. 5; Table 3), according to (i) their experimentally observed coupling constants (Fig. 3); and (ii) their ROESY correlation due to a typical 1,3 diaxial interaction (Fig. 5; Table 5).

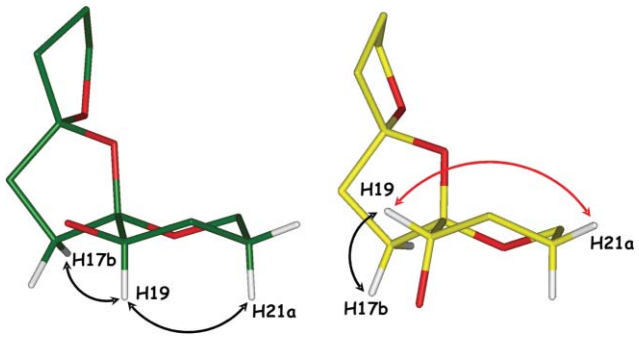

Fig. 5 Lowest energy conformers of the calculated most abundant conformational family of ring F. Left, 4*R*19*R* diastereoisomer; right, 4*R*19*S* diastereoisomer. Hydrogens were omitted, with the exception of those involved in ROESY correlations. Black arrows indicate possible ROEs, red arrows indicate impossible ROEs.

2.4 Identification of the experimentally observed conformations

Once we unambiguously assigned the relative configuration of 13,19-didesmethyl spirolide C, we performed an in-depth analysis of the conformational behavior of **2**, in light of all the NMR parameters dependent upon molecular conformation. To this aim, all of the obtained conformers were ranked by their conformational energies and grouped into families (Table 4; Table S2 in the ESI†) according to the values of the following dihedral angles (named as reported in Fig. 2): (i) β (C5–C6–C7–C29), γ (C5–C35–C34–C29), η (C29–C30–C31–C43), and θ (C28–N–C33–C32), which defined the B- and C-ring conformation; (ii) δ (C29–C7–C8–C9), which defined C38 methyl orientation; (iii) ω (C12–C13–C14–C15), χ, ε, and ζ, which defined the spiro-system conformation (rings D-E-F), and (iv) μ (C9–C10–C11–C12) and ν (C10–C11–C12–C13), related to the rotation along C10–C11 and C11–C12 bonds (see Experimental for details). Finally, all the resulting conformational families were filtered on the basis of our NMR data.

According to the large number of degrees of freedom present in the structure (*i.e.*, rotatable bonds) the analysis yielded a large number of conformational families (Table S2 in the ESI†). Nevertheless, when the conformational results were analyzed taking into account all of the NMR data, it emerged that all conformers within 5 Kcal/mol from the global minimum shared the following conformational features (Table 4. Fig. S1 in the ESI): (i) a *chair* conformation for ring F, characterized by ε ~ −50° and ζ ~ +50°; (ii) a "*pseudo-chair*" conformation ring B, characterized by dihedral angle values β ~ +20° and γ ~ −40°, and (iii) methyl C38 assuming an "*endo*" position, defined by negative values of the dihedral angle δ.

In addition, 50% of conformers within 5 kcal/mol showed ring C conformation (η ~ −160° and θ ~ +60°) consistent with the observed ROESY correlations (Table 5) and 38.5% showed dihedrals μ and ν values (μ ~ 170° and ν ~ −60°) consistent with the experimentally calculated coupling constants (Table 4 and Table 6. Fig. S1 in the ESI†). In particular, $^{3}J_{H\text{-}H}$, $^{2}J_{C\text{-}H}$, and $^{3}J_{C\text{-}H}$ (Table 6 and Fig. 3b) values relative to C10–C11 rotatable bond were consistent only with an *anti* periplanar orientation of C9 with respect to C12 (μ value around 170°; Fig. 6). On the other hand, $^{3}J_{H\text{-}H}$, $^{2}J_{C\text{-}H}$, and $^{3}J_{C\text{-}H}$ values relative to a C11–C12 rotatable bond pointed to a *gauche*-like orientation of C10 with respect to C13 (ν value around −60°; Table 6 and Fig. 7).

Table 6 $^{3}J_{H\text{-}H}$, $^{2}J_{C\text{-}H}$, and $^{3}J_{C\text{-}H}$ values relative to C10–C11 and C11–C12 bonds, respectively, of 13,19-didesmethyl spirolide C

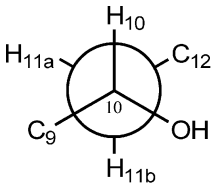

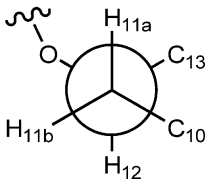

$^{3}J_{H10\text{-}H11a}$	Small	$^{3}J_{H12\text{-}H11a}$	Large
$^{3}J_{H10\text{-}H11b}$	Large	$^{3}J_{H12\text{-}H11b}$	Small
$^{3}J_{H10\text{-}C12}$	Small	$^{3}J_{H12\text{-}C10}$	Small
$^{3}J_{H11a\text{-}C9}$	Small	$^{3}J_{H11a\text{-}C13}$	Small
$^{3}J_{H11b\text{-}C9}$	Small	$^{3}J_{H11b\text{-}C13}$	Large
$^{2}J_{H11a\text{-}C10}$	Small	$^{2}J_{H11a\text{-}C12}$	Large
$^{2}J_{H11b\text{-}C10}$	Large	$^{2}J_{H11b\text{-}C12}$	Large

Homonuclear constants have been evaluated analyzing a z-filtered TOCSY. Heteronuclear coupling constants have been qualitatively assessed by comparison of intensities of cross-peaks in a ps-HMBC spectrum. Displayed dominant conformers have been identified according to the *J*-based configuration method proposed by Murata.[10]

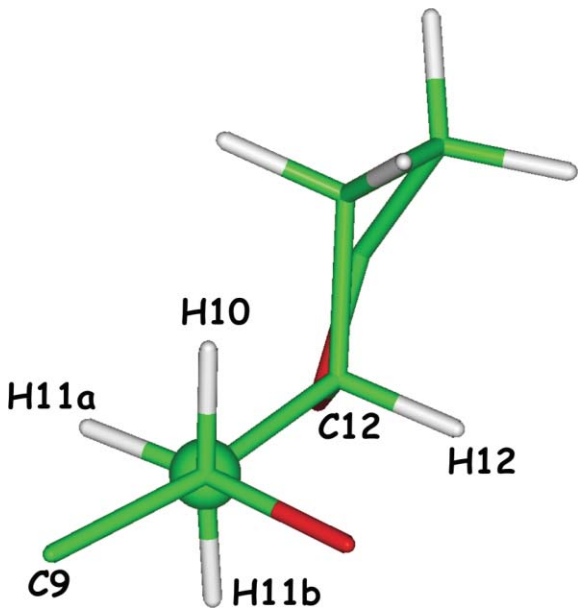

Fig. 6 Anti periplanar orientation of C9 with respect to C12, corresponding to the observed $^{3}J_{H\text{-}H}$, $^{2}J_{C\text{-}H}$, and $^{3}J_{C\text{-}H}$ values for a C10–C11 rotatable bond. Carbon atom C11 is represented by a ball for clarity of presentation.

Interestingly, our analysis evidenced that the observed ROESY cross-peaks between H10 and H13b, as well as between H10 and H14b (Table 5) could not be contemporaneously present, unless two different conformations of ring D (corresponding to $\omega \sim +40°$ and $\omega \sim -40°$; Fig. 7) had been assumed. This result allowed us to hypothesize the existence of a rapid equilibrium in solution between these two ring D conformers.

Finally, we found that both conformations of ring E (corresponding to $\chi \sim +32°$ and $\chi \sim -22°$) were consistent with our NMR data (Fig. 8 and Table 4. Table S2 in the ESI†).

In conclusion, by combining NMR data with computational results, we selected three conformational families, namely family I, II, and IV (Table 4; Table S2 in the ESI†). The structural (heavy atoms) superimposition of the lowest energy conformer

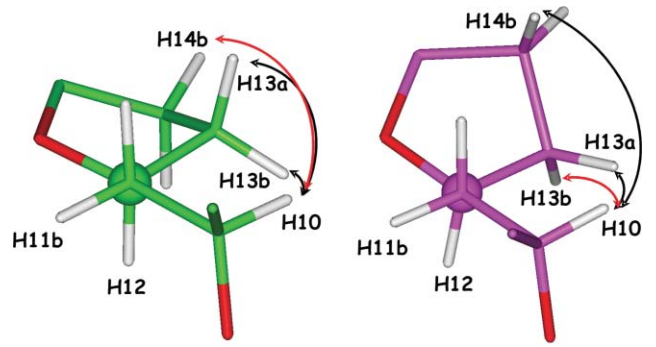

Fig. 7 *Gauche*-like orientation of C10 with respect to C13, corresponding to dihedral angle ν value around –60°. The two conformations of D ring consistent with H10–H13b or H10–H14b ROESY correlations are reported (ω ~ +40°, green; ω ~ –40°, magenta). Carbon atom C12 is represented by a ball for clarity of presentation. Black arrows indicate possible ROEs; red arrows indicate impossible ROEs.

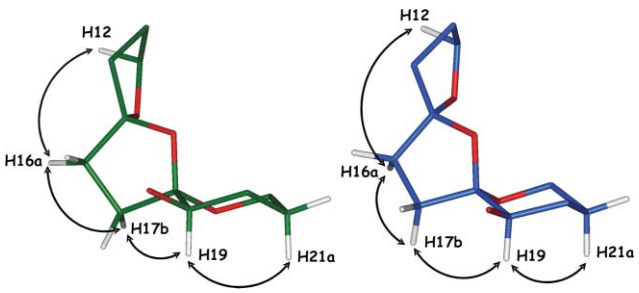

Fig. 8 Calculated ring E conformations, corresponding to $\chi \sim +32°$ (left) and $\chi \sim -22°$ (right). Black arrows indicate possible ROEs.

of each family is reported in Fig. 9. The identified conformers appeared to be differing for the conformation of rings D and E and, by consequence, in the orientation of the exomethylene group at position 41. In particular, they were characterized by the following combination of ring D and E dihedral angle values: $\chi = +32°$, $\omega = +40°$ (family I), $\chi = -22°$, $\omega = +41°$ (family II), $\chi = +33°$ $\omega = -39°$ (family IV). Families I and II, differing only in the ring E conformation, were both consistent with experimental

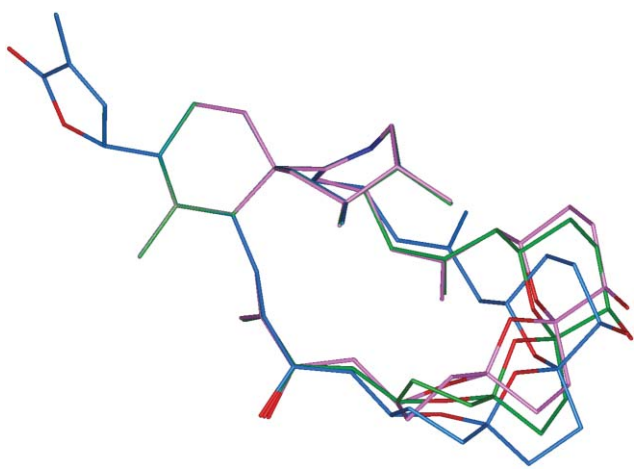

Fig. 9 Superimposition of the identified solution conformations of 13,19-didesmethyl spirolide C: lowest energy conformer of I (green carbons), II (cyan carbons), and IV (pink carbons) families, as reported in Table 4.

data with the exception of the H10/H14b ROESY cross-peak; on the other hand, family IV was in agreement with all NMR data with the exception of the ROE between H10/H13b. It has to be underlined that these conformational families represented 20% of conformers within 5 Kcal/mol from the global minimum, with family I representing the global minimum itself (Table 4; Fig. S1 in the ESI†).

The fourth possible combination of ring D and E dihedral angle values (*i.e.*, negative values of both χ and ω) showed an H-bond between the C10 hydroxyl group and ring E oxygen, causing a distortion of dihedral angles μ and ν. As a consequence, the resulting conformer was not consistent with observed $^{3}J_{H\text{-}H}$, $^{2}J_{C\text{-}H}$, and $^{3}J_{C\text{-}H}$ values relative to C10–C11–C12 rotatable bonds (Table 6; Family XXXVII in Table S2 in the ESI†). This last combination—showing also a $\Delta E_{GM} > 5$ Kcal/mol—was definitively excluded.

In conclusion, our NMR- and molecular modeling-based studies allowed us to identify the existence of an equilibrium in solution among three major conformations of 13,19-didesmethyl spirolide C, as reported in Fig. 9. Interestingly, in all of the three conformations the cyclic imine moiety, which seems to play a key role in spirolide biological activity, always adopted the same conformation.

Experimental

3.1 NMR data

NMR spectra were measured on a Varian Unity Inova 700 spectrometer equipped with a 13C Enhanced HCN Cold Probe. Shigemi 5 mm NMR tubes and CD_3OD as an internal standard (δ_H 3.31 and δ 49.0) were used. *J* values are given in Hz. Standard Varian pulse sequences were employed for the respective classes of spectra; solvent signal suppression by presaturation was used when required. All of the NMR data reported in the text were derived from 2D ^{1}H-^{1}H COSY, z-filtered TOCSY, ROESY, and phase sensitive HMBC spectra.

ROESY was registered at 400 ms mixing time. Cross-peaks were subdivided in 'strong', 'medium', 'weak', and 'very weak' based on the relative peak heights. Strong cross peak were those showing intensity $I > I_{MAX}$, where I_{MAX} represents the most intense peak in the spectrum; medium peaks showed intensities in the range (1/4) I_{MAX} through (1/2) I_{MAX}, weak peaks from (1/8) I_{MAX} through (1/4) I_{MAX}, and very weak peaks with intensities $I < (1/8)\ I_{MAX}$.

3.2 Molecular modeling studies

Molecular modeling calculations were performed on SGI Origin 200 8XR12000, while graphics were carried out on SGI Octane 2 and Octane workstations. Assuming the configuration of previously determined chiral centers as depicted in Fig. 2, in order to unambiguously assign the relative stereochemistry at C4 and C19 atoms, the four possible 13,19-didesmethyl spirolide C diastereoisomers (namely 4*R*19*S*, 4*S*19*R*, 4*R*19*R* and 4*S*19*S*) were built using the Insight 2005 *Builder* module (Accelrys, San Diego). The immino nitrogen of all compounds was considered unprotonated, in accordance with NMR chemical shift data.[2] Molecular mechanics (MM) and dynamics (MD) calculations were performed with the Insight 2005 *Discover_3* module, using the atomic potentials and charges assigned by the CFF91 force field.[11] To simulate the same environment embedding the molecule during the NMR experiments, a distance-dependent dielectric constant was set to the value of methanol (ε = 33*r). The conformational space of these compounds was sampled through 200 cycles of Simulated Annealing, following our standard protocol (*Discover_3* module, Insight 2005). In particular, the system was heated up to 1000 K over 2000 fs (time step = 2.0); the temperature of 1000 K was applied to the system for 2000 fs (time step = 2.0) with the aim of surmounting torsional barriers; successively temperature was linearly reduced to 300 K in 1000 fs (time step = 1.0). Resulting structures were subjected to energy minimization within the Insight 2005 *Discover_3* module (CFF91 force field[a], ε = 33*r), until the maximum RMS derivative was less than 0.001 kcal/Å, using Conjugate Gradient[12] as a minimization algorithm. MD/MM resulting conformers were subjected to a full geometry optimization using quantum-mechanical calculations at semi-empirical AM1 level in the Mopac2007 package[13] and EF (Eigenvector Following routine) as geometry optimization algorithm. The GNORM value was set to 0.01. To reach a full geometry optimization the criteria for terminating all optimizations were increased by a factor of 100, using the keyword PRECISE.

Both the MD/MM conformers and AM1 conformers were ranked on the basis of their conformational energy values and grouped into families according to the following geometric parameters: (a) H4–C4–C5–C6 (namely α), defining the orientation of lactone moiety A with respect to ring B; (b) C5–C6–C7–C29 and C5–C35–C34–C29 (namely β and γ, respectively), defining the cyclohexene ring B conformation; (c) C28–N–C33–C32 and C29–C30–C31–C43 (namely θ and η, respectively), defining the ring C conformation; (d) C18–C19–C20–C21 and C19–C20–C21–C22 (namely ε and ζ, respectively), defining the pyranose ring F conformation; (e) C12–C13–C14–C15 and C15–C16–C17–C18 (namely ω and χ, respectively) defining the tetrahydrofuran (THF) rings D and E conformation; (f) C29–C7–C8–C9 (namely δ) defining the C38 methyl position, and, finally, (g) C9–C10–C11–C12 and C10–C11–C12–C13 (namely μ and ν) defining the C10–C11 and C11–C12 bonds conformation. Families were classified considering a clockwise and counter-clockwise angle increment of 60° in the range of 0°±180° for each dihedral angle. The "*endo*" and "*eso*" methyl C38 positions were identified by negative and positive values of dihedral angle δ, respectively.

We tested the capability of different empirical (MM, CFF91 and CVFF forcefields) and semiempirical (AM1, PM6 and RM1) methods in reproducing the geometry of experimentally determined X-ray structures containing THF-spiro systems. To this aim, we firstly performed a structural search using the *Conquest* software contained in the CSDS[14] (Cambridge Structural Database System) and using as a query the spiro-system present in 13,19-didesmethyl spirolide C. The following structures (CSD codes): (i) ABOHOP, ABOHIJ containing three spiro systems and, (ii) CEFXIV containing two spiro system THF-tetrahydropyran resulted. In all of these structures THF rings presented staggered conformations. ABOHOP, ABOHIJ and CEFXIV structures were optimized with different MM force fields (CVFF and CFF91 forcefield[11]), as well as different QM semiempirical methods (AM1, PM6 and RM1), with the same criteria described above for AM1 calculations. In particular, since ABOHOP and ABOHIJ contained a non-parameterized silicon atom, only CEFXIV was optimized with the semiempirical method AM1.

Results showed that MM, and in particular the CFF91 force-field, was more reliable in reproducing these systems (RMS between our results and X-ray structures calculated on heavy atoms of spiro system: $CFF91_{RMS} < 0.05$ Å; $CVFF_{RMS} < 0.09$ Å). On the contrary, the semiempirical calculations yield flatter geometries, with the AM1 method producing the best results among the semiempirical methods (RMS between our results and CEFXIV X-ray structure calculated on heavy atoms of the bicyclic system: $AM1_{RMS} = 0.25$ Å and $PM6_{RMS} = 0.28$ Å).

Conclusion

The present study based on a combination of NMR techniques and molecular modeling approach offered insightful details on the full relative stereochemistry of spirolides thus far only partially elucidated. Moreover, identification of conformations that 13,19-didesmethyl spirolide C adopts in solution could pave the way for a better understanding of the molecular bases of the biological activity of this class of intriguing marine biotoxins.

Acknowledgements

The authors wish to thank Professor Pistocchi Rossella and Guerrini Franca from the University of Bologna for graciously providing us Adriatic *Alexandrium ostenfeldii* cultures. This work is a result of a research supported by MURST PRIN (2007), Rome, Italy. NMR experiments were performed at the "Centro di Servizi Interdipartimentale di Analisi Strumentale", University of Naples "Federico II", Italy. The assistance of the staff is gratefully appreciated.

References

1 P. Ciminiello, C. Dell'Aversano, E. Fattorusso, S. Magno, L. Tartaglione, M. Cangini, M. Pompei, F. Guerrini, L. Boni and R. Pistocchi, *Toxicon*, 2006, **47**, 597.
2 T. Hu, I. W. Burton, A. D. Cembella, J. M. Curtis, M. A. Quilliam, J. A. Walter and J. L. C. Wright, *J. Nat. Prod.*, 2001, **64**, 308.
3 S. L. MacKinnon, J. A. Walter, M. A. Quilliam, A. D. Cembella, P. LeBlanc, I. W. Burton, W. R. Hardstaff and N. I. Lewis, *J. Nat. Prod.*, 2006, **69**, 983.
4 P. Ciminiello, C. Dell'Aversano, E. Fattorusso, M. Forino, L. Grauso, L. Tartaglione, F. Guerrini and R. Pistocchi, *J. Nat. Prod.*, 2007, **70**, 1878.
5 D. Richard, E. Arsenault, A. D. Cembella and M. A. Quilliam, in *Intergovernmental Oceanographic Commission of UNESCO: Harmful Algal Blooms 2000*, ed. G. M. Hallegraeff, S. I. Blackburn, C. J. Bolch and R. J. Lewis, 2000, p. 383.
6 T. Hu, J. M. Curtis, Y. Oshima, M. A. Quilliam, J. A. Walter, W. M. Watson-Wright and J. L. C. Wright, *J. Chem. Soc., Chem. Commun.*, 1995, **20**, 2159.
7 T. Hu, J. M. Curtis, J. A. Walter and J. L. C. Wright, *Tetrahedron Lett.*, 1996, **37**, 7671.
8 M. Falk, I. W. Burton, T. Hu, J. A. Walter and J. L. C. Wright, *Tetrahedron*, 2001, **57**, 8659.
9 J. A. Dobado, J. Molina Molina and M. Rodriguez Espinosa, *Theochem*, 1994, **109**, 205.
10 M. Murata, S. Matsuoka, N. Matsumori, D. Kaneno, G. K. Paul and K. Tachibana, *J. Am. Chem. Soc.*, 1999, **121**, 870.
11 J. R. Maple, M. J. Hwang, T. P. Stockfisch, U. Dinur, M. Waldman, C. S. Ewig and A. T. Hagler, *J. Comput. Chem.*, 1994, **15**, 162.
12 R. Fletcher, in *Pratical Methods of Optimization*, ed. J. Wiley, & Sons, New York, 1980, vol. 1.
13 MOPAC2007, J. P. James Stewart, *Stewart Computational Chemistry*, Colorado Springs, CO, USA, http://OpenMOPAC.net.
14 I. J. Bruno, J. C. Cole, P. R. Edgington, M. Kessler, C. F. Macrae, P. McCabe, J. Pearson and R. Taylor, *Acta Crystallogr., B*, 2002, **58**, 389.